

# Dye-sensitized solar cells using ethynyl-linked porphyrin trimers<sup>†</sup>

Cite this: *Phys. Chem. Chem. Phys.*,  
2014, 16, 4551

Tomofumi Hamamura,<sup>a</sup> Joanne Ting Dy,<sup>a</sup> Koichi Tamaki,<sup>a</sup> Jotaro Nakazaki,<sup>a\*</sup>  
Satoshi Uchida,<sup>b</sup> Takaya Kubo<sup>a</sup> and Hiroshi Segawa<sup>a\*</sup>

Toward the extension of the light-harvesting region of sensitizers in dye-sensitized solar cells (DSSCs), two ethynyl-linked porphyrin trimers were synthesized and investigated. The zinc-freebase-zinc trimer (**Zn-FbA-Zn**) showed an absorption maximum at a longer wavelength than the all-zinc trimer (**Zn-ZnA-Zn**), although the energy level of **Zn-FbA-Zn** was lower than that of **Zn-ZnA-Zn**. The DSSCs using these trimers showed spectral sensitivities up to 900 nm. Reflecting the energy levels of these trimers, the DSSC using **Zn-ZnA-Zn** showed better performance than that using **Zn-FbA-Zn**. After the optimization of cell fabrication conditions, the photoelectric conversion efficiency  $\eta$  of the DSSC using **Zn-ZnA-Zn** reached 3.17%. The larger  $\text{TiO}_2$  nanoparticles (ca. 37 nm) than the conventional cases (ca. 13 nm) were found to be preferable in this case, due to high molar extinction coefficients of the porphyrin trimers.

Received 9th December 2013,  
Accepted 7th January 2014

DOI: 10.1039/c3cp55184a

[www.rsc.org/pccp](http://www.rsc.org/pccp)

## Introduction

Photo-energy conversion of dye-sensitized solar cells (DSSCs) is based on photo-excitation of sensitizers and following electron transfer reactions.<sup>1–3</sup> For the improvement of the photo-energy conversion efficiency, expansion of the light absorption region of the dyes is important.<sup>4,5</sup> Recently, some DSSCs using porphyrins as the sensitizers have been reported to exhibit relatively high energy conversion efficiency,<sup>6–9</sup> whereas the photoelectric conversion is limited to the visible region. If the spectral sensitivities of the porphyrin-based sensitizers were extended to the near-IR region, the total photoelectric conversion efficiency of DSSCs could be improved. There have been several approaches to make the absorption bands of porphyrins more broad, by extending the  $\pi$ -conjugated systems of porphyrins. In the case of the “fused” approach,  $\pi$ -conjugated systems are extended effectively because of their coplanar structures.<sup>10–14</sup> For example, fused porphyrin dimers show a broad absorption band exceeding 1200 nm.<sup>13</sup> However, such modification of the  $\pi$ -systems of porphyrin causes a large perturbation of their properties. The fused porphyrin dimer showed a low quantum efficiency at the visible region. A large planar compound has a possibility of low solubility in organic

solvents, making the preparation procedures difficult. Another approach to extend  $\pi$ -conjugated systems of porphyrins is the “oligomer” approach. In the case of porphyrin oligomers,<sup>15–20</sup> it had been reported that the intense Soret band absorption became broader along with the increase in the number of porphyrin units. Among several types of porphyrin oligomers, ethynyl-linked porphyrin oligomers are attractive, in view of the effective  $\pi$ -conjugation through rigid ethynyl linkers. The ethynyl linkers are not only rigid but also provide the possibility of rotational motion around the axis, which could lead to a variety of properties based on rotational isomers. Optical properties of porphyrin oligomers have been intentionally documented since each porphyrin unit of the oligomers almost preserves the properties of its monomeric derivatives. Although there were some reports of the DSSCs based on porphyrin dimers,<sup>21–25</sup> the absorption maxima of porphyrin dimers are shorter than 750 nm. Some ethynyl-linked porphyrin trimers<sup>17,20</sup> were reported to show Q band absorption maxima at around 800 nm. Therefore, they could be utilized to achieve photoelectric conversion at the near-IR region. In this study, a zinc porphyrin trimer (**Zn-ZnA-Zn**) and a bis-zinc mono-freebase heteroporphyrin trimer (**Zn-FbA-Zn**) as shown in Fig. 1 have been synthesized to extend the light harvesting region. Freebase porphyrins are favorable for extending the absorption region, while zinc porphyrins are advantageous in the electron releasing reactions. The effect of the combination of these units has been investigated.

## Experimental section

### Synthesis

The synthetic routes of the porphyrin trimers are shown in Scheme 1. The monomeric precursors of the ethynyl-linked

<sup>a</sup> Research Center for Advanced Science and Technology, The University of Tokyo, 4-6-1, Komaba, Meguro-ku, Tokyo 153-8904, Japan.

E-mail: [cnakaz@mail.ecc.u-tokyo.ac.jp](mailto:cnakaz@mail.ecc.u-tokyo.ac.jp); [csegawa@mail.ecc.u-tokyo.ac.jp](mailto:csegawa@mail.ecc.u-tokyo.ac.jp);  
Fax: +81-3-5452-5299; Tel: +81-3-5452-5295

<sup>b</sup> College of Arts and Sciences, The University of Tokyo, 3-8-1, Komaba, Meguro-ku, Tokyo 153-8902, Japan

† Electronic supplementary information (ESI) available: Details of synthetic procedures, DFT calculation results, raw data of electrochemistry, dark current data, and photovoltaic performance data. See DOI: [10.1039/c3cp55184a](https://doi.org/10.1039/c3cp55184a)



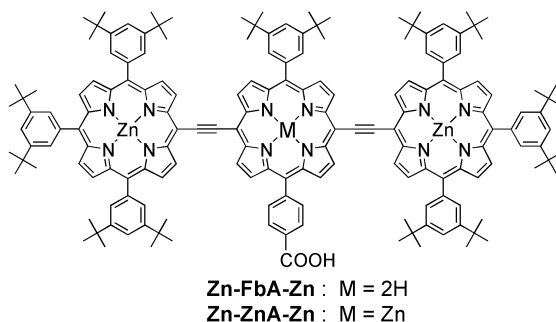


Fig. 1 Structure of the porphyrin trimers used in this study.

porphyrin trimers were synthesized according to previously reported procedures. Sonogashira coupling of **2** and **5** yielded the first trimer **Zn-FbE-Zn**, which was metallated with zinc acetate dihydrate in a methanol–chloroform solution to give the trimer **Zn-ZnE-Zn**. Hydrolysis of the two trimers was achieved by treatment with sodium hydroxide in a methanol–tetrahydrofuran solution to give the target compounds **Zn-FbA-Zn** and **Zn-ZnA-Zn**. The detailed synthetic procedures are described in the ESI.†

### Optical spectroscopy

The UV-visible absorption spectra in solution and on  $\text{TiO}_2$  were recorded on a JASCO V-570 UV/Vis/NIR spectrophotometer. The steady-state fluorescence spectra were recorded on a Shimadzu

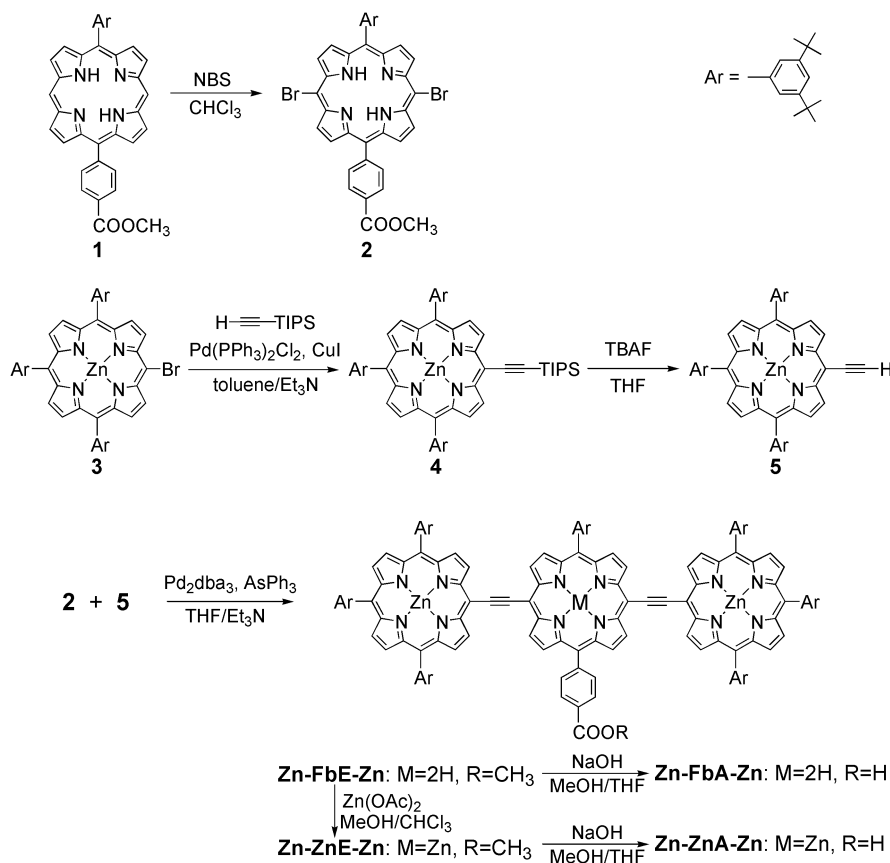
RF-503A difference spectrofluorophotometer. To obtain the absorption spectra of the dyes on  $\text{TiO}_2$ , transparent 3  $\mu\text{m}$ -thick  $\text{TiO}_2$  films were prepared as is described in device fabrication. The absorption of the  $\text{TiO}_2$  film and the substrate was subtracted from the raw spectrum.

### Electrochemistry

Electrochemical measurements were performed by the differential pulse voltammetry (DPV) method on a BAS100 electrochemical analyzer. The voltammograms were recorded under argon flow using a 0.1 M  ${}^{\text{t}}\text{Bu}_4\text{NPF}_6$  in  $\text{CH}_2\text{Cl}_2$  as the supporting electrolyte. A two compartment cell connected by a salt bridge was employed containing the porphyrin solution, a platinum disk (BAS) working electrode and a Pt wire counter electrode in one cell, and an  $\text{Ag}/\text{AgCl}$  reference electrode in a saturated KCl aqueous solution in the other cell. Ferrocene/ferrocenium (0.53 V vs.  $\text{Ag}/\text{AgCl}$ ) was used as the external potentiometric standard. All of the measured values were converted to the potentials vs. SCE.

### Device fabrication

The mesoporous titania films were prepared using commercial pastes of nanoporous anatase  $\text{TiO}_2$  (Ti-Nanoxide, Solaronix) with mean particle sizes of 13 nm and 400 nm for the transparent active layer and the opaque scattering layer, respectively. The pastes were coated by the screen-printing method onto a fluorine-doped  $\text{SnO}_2$  glass plate (FTO, Nippon Sheet Glass). The



Scheme 1 Synthetic routes for the ethynyl-linked porphyrin trimers.



printed  $\text{TiO}_2$  film on glass was sintered at 500 °C for 30 min, treated with  $\text{TiCl}_4$  solution at 70 °C for 30 min, and sintered once more at 500 °C. For the photoanode preparation, the porphyrin dyes were adsorbed on  $\text{TiO}_2$  by immersing the  $\text{TiO}_2$  films into a  $1.0 \times 10^{-5}$  M dye solution in 1:1 chloroform/ethanol (v/v) containing deoxycholic acid (DCA) with various concentrations at 30 °C for 24 h. The films were rinsed with the immersing solvent before use.

For the measurement of absorption spectra, only transparent  $\text{TiO}_2$  nanoparticles were coated on the glass plate, and the film thickness was around 3  $\mu\text{m}$ . In the case of the DCA concentration dependence investigation, both transparent and scattering nanoparticles were used with a total film thickness of 5  $\mu\text{m}$ . For studies on the effect of the  $\text{TiO}_2$  nanoparticle size on the DSSC performance, nanoparticles with mean particle sizes of 13 nm and 37 nm were used to prepare films with thicknesses ranging from 4 to 25  $\mu\text{m}$ .

The DSSC was assembled by injecting the electrolyte between the photoanode and a Pt-coated glass counter electrode (Geomatec). The gap of which was separated by a 30  $\mu\text{m}$  spacer (Himilan, DuPont). The electrolyte was composed of 0.1 M LiI, 25 mM  $\text{I}_2$ , 0.44 M 1,2-dimethyl-3-propylimidazolium iodide (DMPII) in acetonitrile. The active area of the cells used was 0.16  $\text{cm}^2$ .

### Photovoltaic characterization

The photovoltaic properties of the cells were measured with a potentiostat (HSV-100, Hokuto Denko) using an AM 1.5G solar simulator (YSS-80, Yamashita Denso) for illumination. The light intensity was calibrated using a standard silicon cell (BS-520 S/N 235, Bunkoukeiki). The collected data were used to calculate the photoelectric conversion efficiency ( $\eta$ ) according to the following equation:  $\eta = J_{\text{SC}} \times V_{\text{OC}} \times \text{FF}/P_{\text{in}}$  where  $J_{\text{SC}}$  is the short-circuit photocurrent density,  $V_{\text{OC}}$  is the open-circuit voltage, FF is the fill factor and  $P_{\text{in}}$  is the incident radiation power.

The incident photon-to-current conversion efficiency (IPCE) spectra were measured using an IPCE measurement system (SM-250E, Bunkoukeiki). A standard silicon solar cell (SiPD S1337-1010BQ, Bunkoukeiki) was used as the reference and the IPCE values were obtained by comparing the current ratio and the IPCE value of the reference cell at each wavelength.

Electron lifetimes in the DSSCs were estimated by the stepped light induced transient measurement of photo-current and voltage (SLIM-PCV) method,<sup>26</sup> using an Eko Instruments PSL-100 system. Transient response of the open-circuit voltage of the cells was measured by causing a minor change in the intensity of the irradiated laser (635 nm), which was fitted with a single exponential function,  $\exp(-t/\tau_c)$ , where  $t$  and  $\tau_c$  are time and electron lifetime, respectively.

## Results and discussion

### Comparison of trimers with different energy levels

The UV-visible absorption and fluorescence spectra of **Zn-FbE-Zn** and **Zn-ZnE-Zn** in  $\text{CH}_2\text{Cl}_2$  are shown in Fig. 2. The absorption onsets of the synthesized trimers are at 870 nm, which is longer

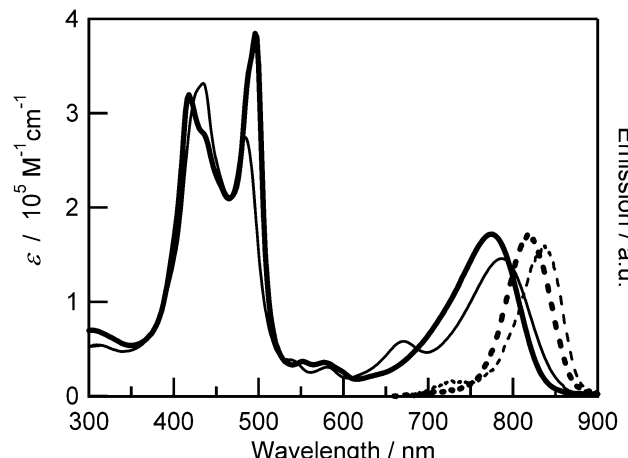


Fig. 2 Absorption (solid line) and emission spectra (dashed line) of **Zn-ZnE-Zn** (thick line) and **Zn-FbE-Zn** (thin line) in  $\text{CH}_2\text{Cl}_2$ .

than that of the monomeric porphyrin (zinc derivative of intermediate compound **1**) by 270 nm. The Q band absorption of the synthesized trimers (around 780 nm) is very intense, with the molar extinction coefficient  $\epsilon$  of more than  $10^5 \text{ M}^{-1} \text{ cm}^{-1}$ , which is 25 times higher than that of the monomeric porphyrin. The absorption maximum in the Q band of **Zn-FbE-Zn** is located at 789 nm, which is longer than that of **Zn-ZnE-Zn** at 778 nm. This is the effect of the freebase porphyrin with smaller excitation energy in **Zn-FbE-Zn**. **Zn-FbE-Zn** has a pronounced peak at 671 nm, which is not seen in **Zn-ZnE-Zn**. A similar Q band spectral shape was also reported for the ethynyl-linked heterometallic porphyrin dimers,<sup>27</sup> and the feature would be attributed to the heterometallic structure. In the short-wavelength region (350–520 nm), Soret (B) band splitting was observed. Such split Soret band has been explained on the basis of the exciton-coupling theory.<sup>28</sup> Fig. 3 illustrates the schemes for the exciton-coupling with a dimer model. Each porphyrin unit of the synthesized trimer has two transition dipole moments ( $\mathbf{B}_x$ ,  $\mathbf{B}_y$ ) in the porphyrin plane. Because of the excitonic coupling between the transition dipole moments along

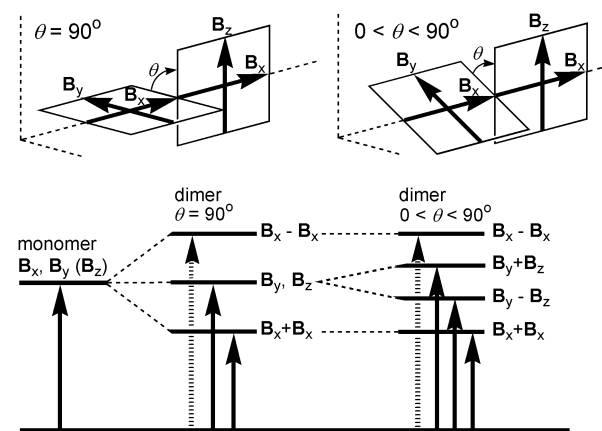


Fig. 3 Schematic drawings for the explanation of split Soret band absorption on the basis of the exciton-coupling theory.

the bonding axis ( $B_x$ ), the excited state is split, and the transition to the excited state with lower energy is allowed, resulting in the red-shifted absorption peak in the Soret band. On the other hand, the excitonic coupling between the transition dipole moments perpendicular to the bonding axis ( $B_y$ ,  $B_z$ ) depends on the dihedral angles between the porphyrin units, affording the shorter wavelength absorption peak. In the observed spectrum, the absorption peak at around 400–450 nm, which is attributed to the transition dipole moments perpendicular to the bonding axis, was broadened. In the case of the trimer with high coplanarity between the adjacent porphyrins, the transition dipole moments are arranged in parallel, leading the blue-shifted absorption derived from the allowed transition to the higher-energy excited state, while the transition dipole moments of the twisted trimer are similar to that of monomeric porphyrins. If the trimers with various dihedral angles exist, they should show the absorption peak at various wavelengths. As a result, the absorption peak would appear broadened. The observed spectra correspond to this consideration. Compared with the Soret band absorption of **Zn-ZnE-Zn**, **Zn-FbE-Zn** showed smaller splitting. The absorption intensity of **Zn-FbE-Zn** at 484 nm ( $\varepsilon \sim 2.75 \times 10^5 \text{ M}^{-1} \text{ cm}^{-1}$ ) was lower than that of **Zn-ZnE-Zn** at 496 nm ( $\varepsilon \sim 3.85 \times 10^5 \text{ M}^{-1} \text{ cm}^{-1}$ ). These features indicate weaker excitonic coupling in the heterometallic trimer. As seen in Fig. 2, the maximum emission of **Zn-FbE-Zn** is located at 836 nm, which is longer than that of **Zn-ZnE-Zn** found at 819 nm. This corresponds to the trend of the Q band absorption peaks and the Stokes shifts (**Zn-ZnE-Zn**: 0.08 eV; **Zn-FbE-Zn**: 0.09 eV) were almost the same.

It has been discussed on the basis of experimental data that the electronic structure of the ethynyl-linked porphyrin trimers depends largely on the dihedral angles between adjacent porphyrin units. To consider such effects, the ethynyl-linked porphyrin trimers without *meso*-substituents were subjected to the DFT calculations (Gaussian 09, B3LYP/6-31G(d)). In the fully optimized structure, the dihedral angle between the central porphyrin and one of the side porphyrins is 33.5°, measured at alpha-*meso*-*meso*-alpha carbons. In this case, the HOMO and the LUMO are distributed over the entire molecule although the coefficients at the central porphyrin are larger than those at the side porphyrins. By freezing the dihedral angles to 90°, the orthogonal conformer was calculated. As shown in Fig. S1 (ESI†), the total energy of the orthogonal conformer is higher than the fully optimized structure by 0.0034 au (0.094 eV). In the orthogonal conformer, the HOMO and the LUMO are localized on the central porphyrin, as shown on the right side of Fig. 4. The degenerated HOMO – 1 and HOMO – 2 are distributed to both the side porphyrins. The LUMO + 1 and the LUMO + 2 are also distributed to both the side porphyrins. Along with the planarization, these orbitals interact, and the energy levels split as shown in the plots in Fig. 4. At the dihedral angle of 5°, the energy level of the HOMO (−4.74 eV) is much higher than that in the orthogonal conformer (−5.15 eV), and the difference in the orbital energies between the HOMO and the corresponding interacted orbital (HOMO – 5) is 0.96 eV. The orbital energy of the LUMO (−2.84 eV) at 5° is lower than

that in the orthogonal conformer (−2.52 eV). The total energy of the conformer with the dihedral angle of 5° is higher than the fully optimized structure by 0.0049 au (0.13 eV). As seen in Fig. S5 (ESI†), the distribution of the LUMO coefficients is similar at the dihedral angles of 10–70°, but the LUMO energies change about 0.2 eV as shown in Fig. 4. Although the extreme dihedral angles, such as 0° or 90°, would not appear at ambient temperatures, the rotation around the ethynyl linkers may affect energetically the performance of these dyes.

To evaluate the energy levels of these dyes, the redox potentials of these trimers were measured by the differential pulse voltammetry (DPV) technique. The voltammograms are shown in Fig. S2 (ESI†), and the obtained redox potentials are summarized in Fig. 5 as the energy-level diagram of these trimers. The oxidation potentials of these trimers are anodic with respect to that of the iodide redox level (+0.2 V vs. SCE). These dyes, thus, have feasible energy levels for the regeneration process of the oxidized dyes by the iodide ions. The reduction potentials of these trimers were cathodic with respect to the TiO<sub>2</sub> conduction band edge potential (−0.7 V vs. SCE) by 0.21 V (**Zn-FbE-Zn**) and 0.52 V (**Zn-ZnE-Zn**), respectively. Considering these potentials, electron injection from the excited **Zn-ZnA-Zn** to TiO<sub>2</sub> is more thermodynamically feasible than that from **Zn-FbA-Zn**.

It should be noted that the oxidation potentials of the excited state is usually used to consider the electron injection. The oxidation potentials of the excited state are estimated from the oxidation potentials of the ground state and the excitation energy  $E_{0-0}$  derived from the fluorescence peak. In the case of **Zn-ZnE-Zn**, the oxidation potential of the excited state was estimated to be −1.04 V (vs. SCE), which is cathodic with respect to the TiO<sub>2</sub> conduction band edge potential by 0.34 V. The oxidation potential of the excited state of **Zn-ZnE-Zn** is anodic with respect to the reduction potential of **Zn-ZnE-Zn** by 0.18 V. As seen here, the reduction potential of **Zn-ZnE-Zn** is much more cathodic with respect to the oxidation potential of the excited state. **Zn-FbE-Zn** is composed of zinc porphyrins as donor units and a freebase porphyrin as an acceptor unit. The first oxidation potential of **Zn-FbE-Zn** would be derived from the zinc porphyrin as a donor unit, while the fluorescence mainly reflects the nature of the freebase porphyrin unit, because the excitation energy of freebase porphyrin is lower than that of zinc porphyrin. Therefore, the estimation of the oxidation potential of the excited state of **Zn-FbE-Zn** using the oxidation potentials of the ground state and excitation energy  $E_{0-0}$  derived from the fluorescence peak is not adequate. To estimate the oxidation potential of the excited state of **Zn-FbE-Zn**, there should be information about the oxidation potential of the freebase porphyrin unit.

In this study, two ethynyl-linked porphyrin trimers with different energy levels, **Zn-ZnA-Zn** and **Zn-FbA-Zn**, are compared. Fig. S3 (ESI†) shows the molecular orbitals of the simplified compounds, all zinc trimer and zinc-freebase-zinc trimer. In these fully optimized structures, the HOMO and the LUMO are distributed over the entire molecule. However, the energy levels of HOMO and LUMO of the zinc-freebase-zinc



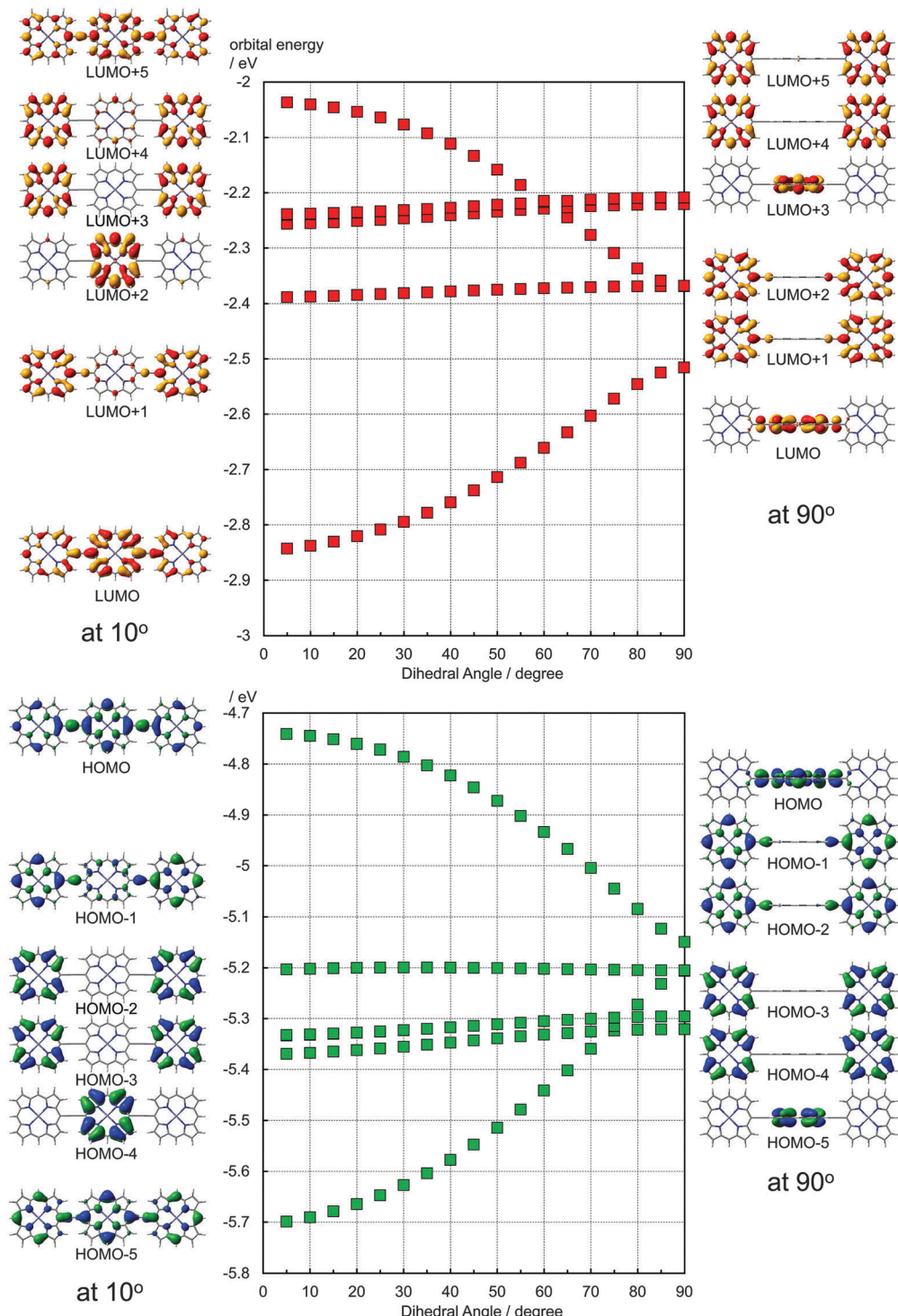
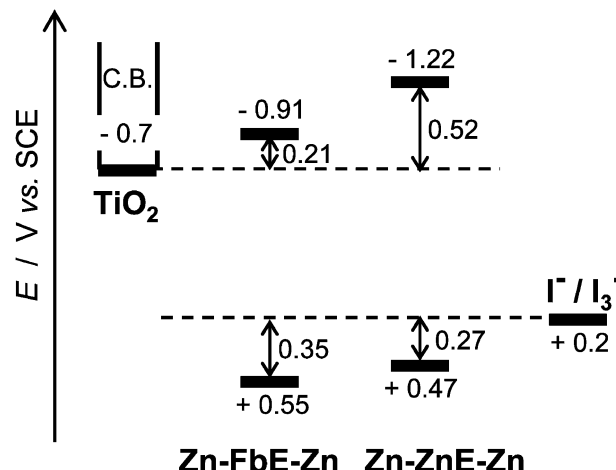


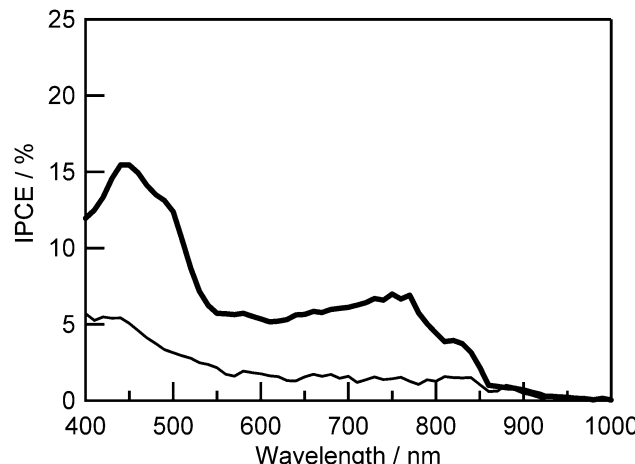
Fig. 4 Calculated orbital energies of ethynyl-linked porphyrin trimers with various dihedral angles and the corresponding molecular orbitals at 10° and 90° by B3LYP/6-31G(d).

trimer are higher than those of the all zinc trimer. This is opposite to the experimental results. It is well known experimentally that freebase porphyrins are electron acceptors in comparison with zinc porphyrins. However, DFT calculations such as B3LYP/6-31G(d) always give the opposite results. Such a tendency has been a barrier for the application of DFT studies

to these derivatives. In some reports, the DFT results which show the distribution of the HOMO at the freebase porphyrin and the distribution of the HOMO-1 at the zinc porphyrin, were presented, although the experimental results are the opposite.<sup>29</sup> In our previous reports on the ethynyl-linked zinc-freebase heteroporphyrin dimer derivatives,<sup>23,24</sup> the HOMO distributed equally at

Fig. 5 Energy-level diagrams of **Zn-FbE-Zn** and **Zn-ZnE-Zn**.

the zinc porphyrin and the freebase porphyrin. These problems could be solved by adopting the solvent effect. There were two reports adopting PCM considerations for the calculation of freebase porphyrins,<sup>30,31</sup> although they didn't mention the improvement of the description for the orbitals of freebase porphyrins. There has also been limitation by the use of the Gaussian03 package. By the appearance of the Gaussian09 package, considerations of the solvent effects using PCM became the regular approach. Recently, phenyl-linked zinc-freebase heteroporphyrin dimers have been calculated, and the importance of the adoption of PCM was confirmed.<sup>32</sup> Since there is still memory limitation for the Gaussian09W package at present, the solvent effect in the DFT study of the ethynyl-linked porphyrin trimers has been investigated using simplified model compounds. Fig. 6 shows the molecular orbitals of the all zinc trimer and the zinc-freebase-zinc trimer without *meso*-substituents, obtained by B3LYP/6-31G(d) employing the solvent effect by CPCM (dichloromethane). Compared to the

Fig. 7 IPCE spectra of DSSCs sensitized with **Zn-ZnA-Zn** (thick line) and **Zn-FbA-Zn** (thin line).  $\text{TiO}_2$  film thickness was 5  $\mu\text{m}$ .

orbitals in Fig. S3 (ESI<sup>†</sup>), the distribution of the HOMO and the LUMO is similar. The orbital energies of the HOMO and the LUMO have, now, the same tendency with the experimental results. By the consideration of the solvent effects, the energy levels of the orbitals related to the freebase porphyrin part are stabilized. In contrast to the reported result on the phenyl-linked dimers,<sup>32</sup> the orbital localization is not seen in the present case. This is the feature of the ethynyl-linked structure. To visualize the solvent effect on the DFT results, the orthogonal conformer of the zinc-freebase-zinc trimer was calculated in vacuum and in dichloromethane (Fig. S4, ESI<sup>†</sup>). It is notable that the HOMO of the zinc-freebase-zinc trimer is distributed on zinc porphyrins under the consideration of the solvent effect, while the HOMO is distributed on freebase porphyrin in vacuum. Since there have been many reports on the properties of freebase porphyrin derivatives, this correction on the DFT results by the consideration of the solvent effect would be important to analyze those data theoretically.

The performances of the DSSCs using these trimers were evaluated. The IPCE spectra of the DSSCs using these trimers are shown in Fig. 7. In the case of **Zn-FbA-Zn**, the IPCE values were less than 3% at the wavelengths from 500 to 900 nm, and less than that of **Zn-ZnA-Zn**. This result reflects the difference in the energy levels. The DSSC using **Zn-ZnA-Zn** showed higher cell performance ( $\eta$ : 0.61%;  $V_{\text{OC}}$ : 0.32 V;  $J_{\text{SC}}$ : 3.17  $\text{mA cm}^{-2}$ ; FF: 0.61) than that of **Zn-FbA-Zn** ( $\eta$ : 0.18%;  $V_{\text{OC}}$ : 0.29 V;  $J_{\text{SC}}$ : 1.10  $\text{mA cm}^{-2}$ ; FF: 0.56). However, even in the case of **Zn-ZnA-Zn**, the IPCE values were just more than 5% at the wavelengths from 500 to 770 nm, although the IPCE spectra increased at around 900 nm.

#### Performances of the DSSCs using **Zn-ZnA-Zn** under various cell fabrication conditions

To improve the cell performance of DSSCs, it is often attempted to reduce the aggregate formation of dyes by the addition of a coadsorbent, such as deoxycholic acid (DCA). The IPCE spectra of the DSSCs using **Zn-ZnA-Zn** with DCA are shown in Fig. 8

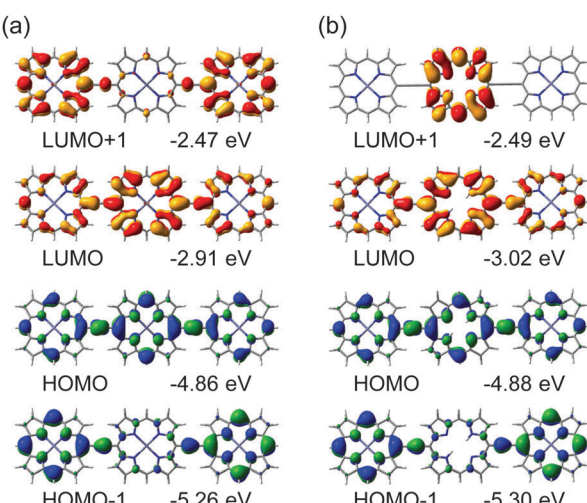
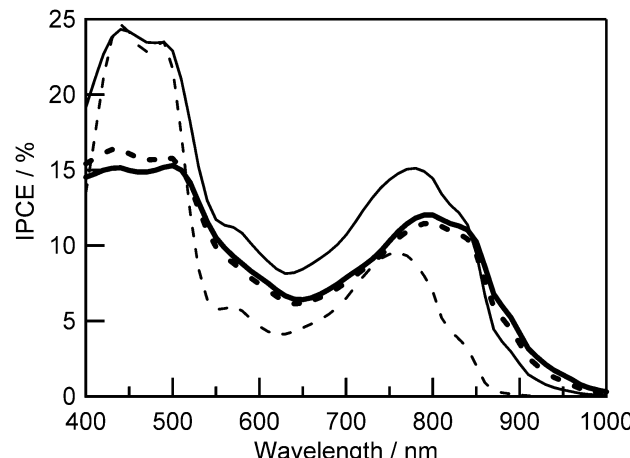
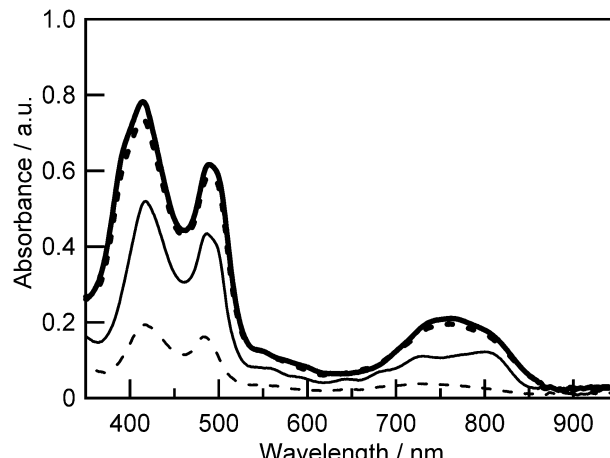


Fig. 6 Molecular orbitals of ethynyl-linked porphyrin trimers calculated by B3LYP/6-31G(d) employing CPCM: (a) all zinc trimer, (b) zinc-freebase-zinc trimer.





**Fig. 8** IPCE spectra of DSSCs sensitized with **Zn-ZnA-Zn** using  $1.0 \times 10^{-5}$  M solution of the dye in 1:1 (v/v)  $\text{CHCl}_3$ –EtOH without a coadsorbent (thick solid line), with  $1.0 \times 10^{-5}$  M DCA (thick dashed line), with  $1.0 \times 10^{-4}$  M DCA (thin solid line) and with  $1.0 \times 10^{-3}$  M DCA (thin dashed line).  $\text{TiO}_2$  film thickness was 5  $\mu\text{m}$ .



**Fig. 9** Absorption spectra of **Zn-ZnA-Zn** on  $\text{TiO}_2$  films using  $1.0 \times 10^{-5}$  M solution of the dye in 1:1 (v/v)  $\text{CHCl}_3$ –EtOH without a coadsorbent (thick solid line), with  $1.0 \times 10^{-5}$  M DCA (thick dashed line), with  $1.0 \times 10^{-4}$  M DCA (thin solid line) and with  $1.0 \times 10^{-3}$  M DCA (thin dashed line).  $\text{TiO}_2$  film thickness was 3  $\mu\text{m}$ .

**Table 1** Photovoltaic properties of DSSCs based on **Zn-ZnA-Zn** with various concentrations of DCA

DCA concentration	$V_{\text{OC}}$ /V	$J_{\text{SC}}$ /mA $\text{cm}^{-2}$	FF	$\eta$ /%
Without DCA	0.442	4.13	0.622	1.14
$1.0 \times 10^{-5}$ M	0.458	4.07	0.622	1.16
$1.0 \times 10^{-4}$ M	0.502	5.22	0.626	1.64
$5.0 \times 10^{-4}$ M	0.558	5.47	0.641	1.96
$1.0 \times 10^{-3}$ M	0.558	3.57	0.642	1.28

and the corresponding photovoltaic properties are listed in Table 1. As shown in Fig. 8, the addition of  $1.0 \times 10^{-5}$  M DCA caused the higher IPCE values than the case without DCA. The addition of  $1.0 \times 10^{-4}$  M DCA caused further improvement, while the addition of  $1.0 \times 10^{-3}$  M DCA caused the decrease in IPCE.

The effect of DCA addition appeared in the absorption spectra, as shown in Fig. 9. In the Q band region, the absorption peak of **Zn-ZnA-Zn** (762 nm) on  $\text{TiO}_2$  was blue shifted with respect to that in 1/1  $\text{CHCl}_3$ –EtOH (v/v) (782 nm) by 20 nm (Fig. S5, ESI†). This blue shift has been caused by the formation of H-type (stacked) aggregates of trimers on the  $\text{TiO}_2$  surface. The absorption intensity of **Zn-ZnA-Zn** with DCA on  $\text{TiO}_2$  decreased along with the increase of the concentration of DCA in the solution of **Zn-ZnA-Zn** due to the decrease of immobilized trimers on the  $\text{TiO}_2$  surface because the coadsorbent also occupied space on the  $\text{TiO}_2$ . The absorption peak at around 700–850 nm was located at a longer wavelength in the case of trimers with DCA. Upon a closer inspection, this spectral change is actually the decrease of the peak intensity at 720 nm relative to the peak at 820 nm as DCA concentration was increased. This result suggests that the addition of DCA suppressed the formation of the H-type aggregates.

The suppression of H-type aggregates is in accord with the improvement of IPCE upon the addition of  $1.0 \times 10^{-5}$  M or  $1.0 \times 10^{-4}$  M of DCA. When the concentration of DCA was

$1.0 \times 10^{-3}$  M, the IPCE values were lower than the other cases with different DCA concentrations. This may be due to the reduction of the amount of dye adsorption. However, the spectral shape in the Q band region showed opposite behavior in comparison with the absorption spectra. The IPCE peak of the DSSC using **Zn-ZnA-Zn** with DCA appeared at a shorter wavelength than that without DCA. In the case of the DSSC using **Zn-ZnA-Zn** without DCA, some portions of dyes are not included in H-type aggregates, and are working for photoelectric conversion. The major portions of dyes form H-type aggregates and work as masks at the shorter wavelength region, leaving the IPCE peak at the longer wavelength region. Therefore, the IPCE values at the Soret band region are low and comparable to those at the Q band region. Along with the increase of the DCA addition, the formation of H-type aggregates is suppressed, reducing the mask effect. Together with the decrease of the total amount of the immobilized trimers on the  $\text{TiO}_2$  surface, the IPCE spectral shape becomes similar to that of the absorption spectra.

As seen in Table 1, the  $J_{\text{SC}}$  values of these DSSCs corresponded to the trends of the IPCE spectra. The  $V_{\text{OC}}$  values of the DSSCs using **Zn-ZnA-Zn** without DCA and those with  $1.0 \times 10^{-5}$  M DCA were similar, within the variation of the measured cells. By further addition of DCA, the  $V_{\text{OC}}$  values increased, but the  $V_{\text{OC}}$  values of those with  $5.0 \times 10^{-4}$  M DCA and  $1.0 \times 10^{-3}$  M DCA were within the variation of the cells. FF values were almost constant regardless of DCA concentrations. As a result, the energy conversion efficiency  $\eta$  was the highest when  $5.0 \times 10^{-4}$  M DCA was added. Several factors have been considered for the cause of the  $V_{\text{OC}}$  variation, such as the dipole moments of the adsorbed dyes on the  $\text{TiO}_2$  surface,<sup>33,34</sup> and the interfacial charge recombination between the electrons in the  $\text{TiO}_2$  conduction band and the redox couple in the electrolyte or the oxidized dyes. To consider the charge recombination rate in these DSSCs, the current–voltage characteristic of the DSSCs

using **Zn-ZnA-Zn** in the dark was measured (Fig. S6, ESI†). The dark current of the DSSCs decreased along with the increase in the DCA concentrations. This fact indicates that the rate of the interfacial charge recombination between the electrons in the  $\text{TiO}_2$  conduction band and the redox couple in the electrolyte is lowered by the addition of DCA. It is suggested that the sufficient DCA coverage over the  $\text{TiO}_2$  surface prevents the charge recombination from the electrons in the  $\text{TiO}_2$  conduction band to  $\text{I}_3^-$ . For further investigation, the electron lifetime of the DSSCs was estimated from the transient photovoltage decay.<sup>24</sup> The data shown here were obtained from the cells used to get the data in Table 1. From the results obtained by changing the light intensity, the electron lifetime was plotted *versus* the  $V_{\text{OC}}$  of the DSSCs at various DCA concentrations (Fig. 10). Basically, the results also show that the charge recombination rate is lower for the high concentration of DCA than for the low concentration. The trend in the electron lifetime data is in better agreement with that of the  $V_{\text{OC}}$ . In the case of the dark current data, the value decreased monotonously along with the addition of DCA, while the  $V_{\text{OC}}$  showed saturation-like behavior. In the plots in Fig. 10, the higher  $V_{\text{OC}}$  correspond to the higher intensity of illumination and the lower  $V_{\text{OC}}$  correspond to weak illumination. The difference in the electron lifetime between the cells with  $5.0 \times 10^{-4}$  M DCA and  $1.0 \times 10^{-3}$  M DCA becomes larger at the weak illumination side, connecting the data in the dark and those under 1 sun illumination. The different ratio of **Zn-ZnA-Zn** and DCA on the  $\text{TiO}_2$  surface caused such behavior.

The low IPCE indicates the possibility that the light-harvesting of the DSSCs is not enough, although the  $\text{TiO}_2$  films for DSSCs were equipped with the scattering layer. In Fig. 9, it is shown that 76% (without DCA) or 37% (with  $1.0 \times 10^{-4}$  M DCA) of photons were absorbed at 490 nm. When such thin  $\text{TiO}_2$  films were used to fabricate DSSCs, the observed IPCE at 490 nm was 15% or 11%, respectively. The internal quantum efficiency (absorbed photon-to-current conversion efficiency, APCE) is

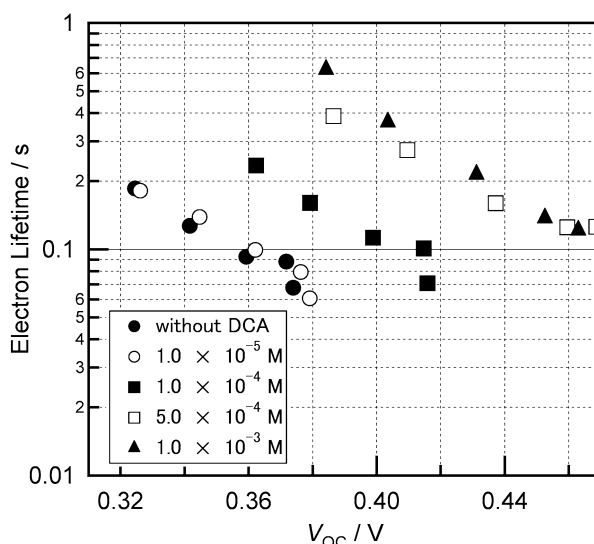


Fig. 10 Electron lifetimes measured under different illumination intensities as a function of open-circuit voltage for the DSSCs with various concentrations of DCA.

roughly estimated to be 20% (without DCA) or 30% (with DCA), respectively. Therefore, the main loss was caused by the low internal quantum efficiency. However, it would be easier to increase the absorption than to improve the internal quantum efficiency. To increase the amount of adsorbed dye, the properties of the DSSCs using **Zn-ZnA-Zn** were investigated for various  $\text{TiO}_2$  film thicknesses and the relevant performance parameters were plotted *versus* the  $\text{TiO}_2$  film thickness in Fig. 11. The  $V_{\text{OC}}$  decreased along with the increase of the film thickness. The  $J_{\text{SC}}$  showed a maximum value at a mean film thickness of 10.6  $\mu\text{m}$ . The FF was constant regardless of the  $\text{TiO}_2$  film thickness. Reflecting these parameters, the  $\eta$  of the DSSCs based on **Zn-ZnA-Zn** showed the highest value of 3.17% ( $V_{\text{OC}}$ : 0.49 V;  $J_{\text{SC}}$ : 10.8  $\text{mA cm}^{-2}$ ; FF: 0.60) under the condition of 10  $\mu\text{m}$  film thickness. The  $V_{\text{OC}}$  decreased significantly along with the

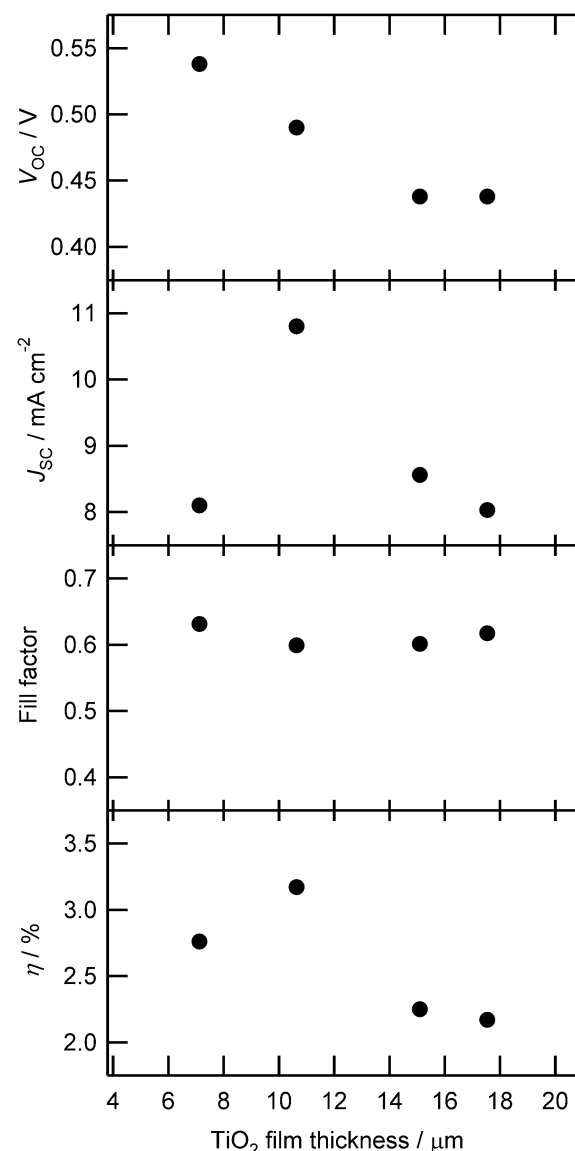


Fig. 11 Dependence of DSSC parameters [open circuit voltage ( $V_{\text{OC}}$ ), current density ( $J_{\text{SC}}$ ), fill factor, and efficiency ( $\eta$ )] sensitized with **Zn-ZnA-Zn** on  $\text{TiO}_2$  film thickness.



increase in the  $\text{TiO}_2$  film thickness as shown in Fig. 11. To consider the charge recombination rate in these DSSCs, the current–voltage characteristic of the DSSCs using **Zn–ZnA–Zn** in the dark was also measured (Fig. S7, ESI†). The dark current of the DSSCs increased along with the increase in the film thickness of  $\text{TiO}_2$ , indicating that the rate of the interfacial charge recombination is larger for thick films than for thin films. The result of the electron lifetime measurements (Fig. S8, ESI†) also shows that the charge recombination rate is faster for thick films than for thin films. From these results, we concluded that the decrease of  $V_{\text{OC}}$  in thicker films was caused by the increase in the charge recombination rate along with the increase in the  $\text{TiO}_2$  film thickness.

Since the long-axis length of the ethynyl-linked porphyrin trimer is about 3 nm, which is comparable to the size of  $\text{TiO}_2$  nanoparticles, the difference in the particle size may affect the adsorption behavior of the ethynyl-linked porphyrin trimer on the  $\text{TiO}_2$  surface. Therefore, the properties of the DSSCs using **Zn–ZnA–Zn** were investigated for two sizes of  $\text{TiO}_2$  nanoparticles (13 nm and 37 nm). The photoelectric conversion efficiencies  $\eta$  were plotted *versus* the  $\text{TiO}_2$  film thickness in Fig. 12, and the other photovoltaic performance parameters are shown in Fig. S9 (ESI†). The  $V_{\text{OC}}$  values of the DSSCs using large particles (37 nm) were constant regardless of the  $\text{TiO}_2$  film thickness, while that of small particles (13 nm) decreased along with the increase of the film thickness. Concerning the  $J_{\text{SC}}$ , the DSSCs composed of small  $\text{TiO}_2$  nanoparticles showed higher values than large particles at the thinner film thickness. This would be caused by the larger specific surface area of the  $\text{TiO}_2$  films composed of small particles than that of large particles. The  $J_{\text{SC}}$  showed maximum values at a certain film thickness: 12  $\mu\text{m}$  for small particles and 20  $\mu\text{m}$  for large particles. The FF was constant regardless of the size of  $\text{TiO}_2$  nanoparticles. Reflecting these parameters, the  $\eta$  of the DSSCs based on **Zn–ZnA–Zn** showed maximum values, and the highest value of 2.25% ( $V_{\text{OC}}$ : 0.48 V;  $J_{\text{SC}}$ : 7.28  $\text{mA cm}^{-2}$ ; FF: 0.64) was obtained

under the conditions of large particle size (37 nm) and 20  $\mu\text{m}$  film thickness. As seen here, larger  $\text{TiO}_2$  particles may be more appropriate as the transparent semiconductor scaffold in DSSCs utilizing large-sized molecules.

## Conclusions

The DSSCs using ethynyl-linked porphyrin trimers (**Zn–FbA–Zn**, **Zn–ZnA–Zn**) showed the spectral sensitivities that increased at around 900 nm, which is a relatively long wavelength among the reported DSSCs based on porphyrins. Among these trimers, **Zn–ZnA–Zn** showed better performance because of its more suitable energy level matching than **Zn–FbA–Zn**. Through the DFT calculations, it was indicated that the energy levels might be changed by the rotational motion along the ethynyl linkers. However, the calculated energy levels matched with the experimental results only when the solvent effect was considered with the CPCM method. To explain the experimental results on the basis of the molecular orbitals, careful considerations are still needed. Since rotational isomers are one of the features of ethynyl-linked porphyrin oligomers, investigations on the contribution of such rotational isomers should be interesting. During the optimization of DSSC fabrication, the thicker  $\text{TiO}_2$  film to increase the surface-adsorbed trimers did not give rise to higher photocurrent, indicating that **Zn–ZnA–Zn** is suitable for the thinner  $\text{TiO}_2$  films. The larger  $\text{TiO}_2$  nanoparticles than the conventional cases were found to be preferable in this case, reflecting the large molecular size of the porphyrin trimer. These results show that ethynyl-linked porphyrin trimers would be one of the promising candidates as a sensitizer with intense and broad absorption for efficient DSSCs. The present results also indicate that the suppression of the aggregate formation without decrease in the amount of surface-adsorbed dyes is requested in this case, because the light-harvesting efficiency is still not enough in spite of the high molar extinction coefficient of the trimer. Since the internal quantum efficiency was about 30% at present, both the light-harvesting efficiency and the internal quantum efficiency should be improved with almost equal weight. Modification of the anchoring groups for such improvements is on the way.

## Acknowledgements

This work was supported by Funding Program for World-Leading Innovative R&D on Science and Technology (FIRST program) on the development of organic photovoltaics toward a low-carbon society, from the Japanese Government, and the Research Fellowships of the Japan Society for the Promotion of Science (JSPS) for Young Scientists.

## Notes and references

- 1 B. O'Regan and M. Grätzel, *Nature*, 1991, **353**, 737.
- 2 M. Grätzel, *Acc. Chem. Res.*, 2009, **42**, 1788.

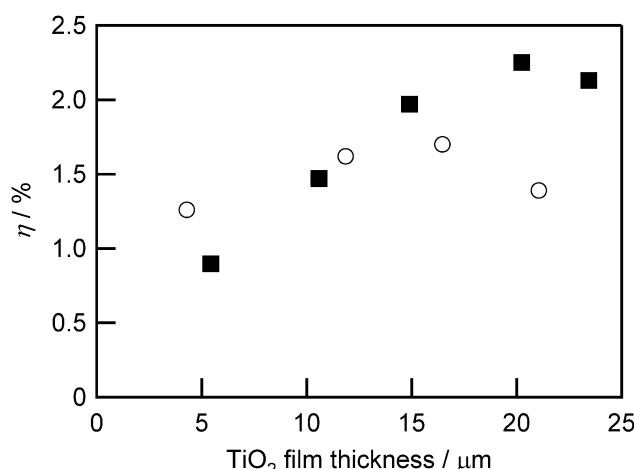


Fig. 12 Dependence of photoelectric conversion efficiency ( $\eta$ ) on  $\text{TiO}_2$  film thickness for cells using 13 nm (open circles) and 37 nm (filled squares)  $\text{TiO}_2$  nanoparticles and sensitized with **Zn–ZnA–Zn**.

3 A. Hagfeldt, G. Boschloo, L. Sun, L. Kloo and H. Pettersson, *Chem. Rev.*, 2010, **110**, 6595.

4 T. Kinoshita, J. Fujisawa, J. Nakazaki, S. Uchida, T. Kubo and H. Segawa, *J. Phys. Chem. Lett.*, 2012, **3**, 394.

5 T. Kinoshita, J. T. Dy, S. Uchida, T. Kubo and H. Segawa, *Nat. Photonics*, 2013, **7**, 535.

6 C.-W. Lee, H.-P. Lu, C.-M. Lan, Y.-L. Huang, Y.-R. Liang, W.-N. Yen, Y.-C. Liu, Y.-S. Lin, E. W.-G. Diau and C.-Y. Yeh, *Chem.-Eur. J.*, 2009, **15**, 1403.

7 T. Bessho, S. M. Zakeeruddin, C.-Y. Yeh, E. W.-G. Diau and M. Grätzel, *Angew. Chem., Int. Ed.*, 2010, **49**, 6646.

8 A. Yella, H.-W. Lee, H. N. Tsao, C. Yi, A. K. Chandiran, M. K. Nazeeruddin, E. W.-G. Diau, C.-Y. Yeh, S. M. Zakeeruddin and M. Grätzel, *Science*, 2011, **334**, 629.

9 L.-L. Li and E. W.-G. Diau, *Chem. Soc. Rev.*, 2013, **42**, 291.

10 S. Hayashi, M. Tanaka, H. Hayashi, S. Eu, T. Umeyama, Y. Matano, Y. Araki and H. Imahori, *J. Phys. Chem. C*, 2008, **112**, 15576.

11 H. Imahori, T. Umeyama and S. Ito, *Acc. Chem. Res.*, 2009, **42**, 1809.

12 A. Kira, Y. Matsubara, H. Iijima, T. Umeyama, Y. Matano, S. Ito, M. Niemi, N. V. Tkachenko, H. Lemmettyinen and H. Imahori, *J. Phys. Chem. C*, 2010, **114**, 11293.

13 C.-L. Mai, W.-K. Huang, H.-P. Lu, C.-W. Lee, C.-L. Chiu, Y.-R. Liang, E. W.-G. Diau and C.-Y. Yeh, *Chem. Commun.*, 2010, **46**, 809.

14 C. Jiao, N. Zu, K.-W. Huang, P. Wang and J. Wu, *Org. Lett.*, 2011, **13**, 3652.

15 D. Kim and A. Osuka, *J. Phys. Chem. A*, 2003, **42**, 8791.

16 D. Kim and A. Osuka, *Acc. Chem. Res.*, 2004, **37**, 735.

17 V. S.-Y. Lin, S. G. DiMagno and M. J. Therien, *Science*, 1994, **264**, 1105.

18 V. S.-Y. Lin and M. J. Therien, *Chem.-Eur. J.*, 1995, **1**, 645.

19 K. Susumu and M. J. Therien, *J. Am. Chem. Soc.*, 2002, **124**, 8550.

20 T. V. Duncan, K. Susumu, L. E. Sinks and M. J. Therien, *J. Am. Chem. Soc.*, 2006, **128**, 9000.

21 J. T. Dy, K. Tamaki, Y. Sanehira, J. Nakazaki, S. Uchida, T. Kubo and H. Segawa, *Electrochemistry*, 2009, **77**, 206.

22 J. K. Park, J. Chen, H. R. Lee, S. W. Park, H. Shinokubo, A. Osuka and D. Kim, *J. Phys. Chem. C*, 2009, **113**, 21956.

23 Y. Liu, H. Lin, J. T. Dy, K. Tamaki, J. Nakazaki, D. Nakayama, S. Uchida, T. Kubo and H. Segawa, *Chem. Commun.*, 2011, **47**, 4010.

24 Y. Liu, H. Lin, J. Li, J. T. Dy, K. Tamaki, J. Nakazaki, D. Nakayama, C. Nishiyama, S. Uchida, T. Kubo and H. Segawa, *Phys. Chem. Chem. Phys.*, 2012, **14**, 16703.

25 H.-P. Wu, Z.-W. Ou, T.-Y. Pan, C.-M. Lan, W.-K. Huang, H.-W. Lee, N. M. Reddy, C.-T. Chen, W.-S. Chao, C.-Y. Yeh and E. W.-G. Diau, *Energy Environ. Sci.*, 2012, **5**, 9843.

26 S. Nakade, T. Kanzaki, Y. Wada and S. Yanagida, *Langmuir*, 2005, **21**, 10803.

27 R. Shediac, M. H. B. Gray, H. T. Uyeda, R. C. Johnson, J. T. Hupp, P. J. Angiolillo and M. J. Therien, *J. Am. Chem. Soc.*, 2000, **122**, 7017.

28 M. Kasha, H. R. Rawls and M. A. El-Bayoumi, *Pure Appl. Chem.*, 1965, **11**, 371.

29 G. Pognon, J. A. Wytko, P. D. Harvey and J. Weiss, *Chem.-Eur. J.*, 2009, **15**, 524.

30 R. Improta, C. Ferrante, R. Bozio and V. Barone, *Phys. Chem. Chem. Phys.*, 2009, **11**, 4664.

31 N. S. Venkataraman, A. Suvitha, H. Nejo, H. Mizuseki and Y. Kawazoe, *Int. J. Quantum Chem.*, 2011, **111**, 2340.

32 T. Tsuchiya and E. Jakubikova, *J. Phys. Chem. A*, 2012, **116**, 10107.

33 S. Rühle, M. Greenshtein, S.-G. Chen, A. Merson, H. Pizem, C. S. Sukenik, D. Cahen and A. Zaban, *J. Phys. Chem. B*, 2005, **109**, 18907.

34 S. S. Pandey, K.-Y. Lee, A. Hayat, Y. Ogomi and S. Hayase, *Jpn. J. Appl. Phys.*, 2011, **50**, 06GF08.

